Research Article Vol. 31, No. 2 / 16 Jan 2023 / Optics Express 1629
Optics EXPRESS

Unconventional photon blockade in a non-Hermitian indirectly coupled resonator system

KAI WANG,[1,2] HENG WANG,[1,2] YONG-PAN GAO,[3] DAQUAN YANG,[4] RONG-ZHEN JIAO,[1,2] AND CHUAN WANG[5,6,*]

[1]School of Science, Beijing University of Posts and Telecommunications, Beijing, 100876, China
[2]The State Key Laboratory of Information Photonics and Optical Communications, Beijing University of Posts and Telecommunications, Beijing 100876, China
[3]School of Electronics Engineering, Beijing University of Posts and Telecommunications, Beijing, 100876, China
[4]School of Information and Communication Engineering, Beijing University of Posts and Telecommunications, Beijing 100876, China
[5]School of Artificial Intelligence, Beijing Normal University, Beijing, 100875, China
[6]Applied Optics Beijing Area Major Laboratory, Beijing Normal University, Beijing 100875, China
*wangchuan@bnu.edu.cn

Abstract: Photon blockade provides an effective way to realize the single-photon source, which attracts intensive attention in the fields of quantum optics and quantum information. Here in this study, we investigate photon blockade in a non-Hermitian indirectly coupled resonator system, which consists of a dissipative cavity and a Kerr nonlinear resonator coupled to two nano-scatters. We find that by tuning the coupling phase θ between the two resonators, the quantum interference could be induced on one side near the exceptional points (EPs), resulting in the unconventional photon blockade effect. Furthermore, it is noticed that the large Kerr nonlinearity is not always beneficial for unconventional photon blockades. There is an optimal threshold for the intensity of the Kerr nonlinearity and the phase angle θ for the appearance of the unconventional photon blockade effect. We believe the current study has substantial consequences for investigating the physical characteristics close to EPs and presents a novel method for developing integrated on-chip single-photon sources.

1. Introduction

Photon blockade is to define a nonclassical anti-bunching effect that satisfies the sub-Poissonian statistics. It plays an important role in the generation and manipulation of single photons, which may be further used in quantum information science. Imamoğlu et al. first proved that photon blockade effect could be generated in the Kerr nonlinear cavity [1]. Subsequently, researchers began to focus on the realization of photon blockade in various physical systems [2–16]. Whispering-gallery-mode (WGM) microcavity is an on-chip device that describes the dielectric structure where light waves are confined by total internal reflection in the microstructure, and light is reflected back on the same optical path where they interfere constructively. Recently, the WGM microcavity has attracted much attention in the field of nanophotonics and quantum optics. As an integrated on-chip optical element, it has a relatively higher quality factor, and small mode volume [17–25], which significantly reduces the threshold of nonlinear effects and been widely used in basic studies of quantum optics [26–28], telecommunications [29–32], and optical sensing [33–35].

In addition, due to the geometric and coupling properties of the WGM microcavity, it is easy to construct two or more coupled systems, for example, the photonic molecules (PMs) [36,37]. During the past decades, the emergence of PMs has opened up a new platform for

#477662 https://doi.org/10.1364/OE.477662
Journal © 2023 Received 7 Oct 2022; revised 26 Nov 2022; accepted 11 Dec 2022; published 5 Jan 2023

Optics EXPRESS

fundamental optics and quantum simulations. Generally, two or more resonators are employed to construct the PMs through the direct coupling by the evanescent field, in which the supermodes could be generated by the superposition of the modes in each resonator. For example, in such directly coupled resonators system, fascinating phenomena could be observed, such as the electromagnetically induced transparency [38,39], the photon blockade [40], and the programmable photonic molecules [41]. Alternatively, there is another way to construct the PMs by using the indirectly coupled optical waveguides [42–45]. The indirect coupling enables the phase controlling of photons between neighboring resonators. In 2012, Li et al. experimentally obtained the adjustable Fano resonance in a whispering gallery microcavity using indirect coupling [46].

In quantum mechanics, the physical system is usually defined as the Hermitian system with real energy spectra. However, due to the dissipation of the system with the environment, the properties of the Hermiticity could be broken, and the system turns to be non-Hermitian. Currently, the studies of non-Hermitian coupled resonators system have attracted intensive attention. For example, in 2020, Peng et al. investigated that the levels of attraction could be observed in the non-Hermitian indirectly coupled systems [47]. In non-Hermitian systems, the eigenvalues and eigenvectors degenerate at EPs, which display sensitive physical features [48–54]. Therefore, the study of indirectly coupled resonant systems combined with non-Hermitian systems is of great significance.

As there is large optical sensitivity of the evanescent fields, it is possible to utilize nano-scatterers on the surface of the WGM resonator to generate the asymmetric coupling between the clockwise (CW) and the counterclockwise (CCW) modes in the microcavity. Therefore, a non-Hermitian system could be observed [55–58]. Recently, Lü et al. studied optomechanically induced transparency in an optomechanical system and realized the conversion between the fast and slow light [59]. Xu et al. studied the controllable generation of high-order sidebands, and frequency combs in cavity optomagnonics [60]. Huang et al. investigated the photon blockade at EPs in a Kerr nonlinear cavity [61]. These studies have uncovered various novel phenomena distinct from the Hermitian system. After integrating an indirectly linked resonator system, Wang et al. discovered that the phase angle of the coupling between two adjacent resonators is strongly connected to the electromagnetically induced transparency [62].

In this study, we investigate the photon blockade in the non-Hermitian indirectly coupled resonators system. Compared with the previous works, the current scheme could manipulate the photon generation process and promote the performance of a single photon source which is the essential device for developing quantum communication and quantum information processing. Traditionally, the photon blockade effect can be generally divided into the conventional photon blockade effect [2–8] and the unconventional photon blockade effect [9–15]. The former depends on the strong nonlinearities in the medium, while the latter depends on the destructive interference between the pathways of photons in the nonlinear systems. Here we mainly focused on the unconventional photon blockade effect in the system and studied the performance of the photon statistical characteristics caused by the phase θ around the EPs. In addition, we find an optimal threshold of the nonlinear strength and the phase θ that may induce the unconventional photon blockade effect. We believe this work is experimentally feasible as it is compatible with current micro-scale manufacturing technologies. It also eliminates the requirement for bulky tunable lasers and may be further applied to the on-chip integrated single-photon sources.

2. Theoretical model

As illustrated in Fig. 1, the indirectly coupled resonator system is a non-Hermitian system that consists of a Kerr nonlinear resonator with two nanotips on the surface and a dissipative cavity. The two cavities are coupled indirectly through an optical waveguide. In addition, the phase θ of the optical waveguide may be tuned by the propagation of an electromagnetic field, a magnetic

Optics EXPRESS

field after coating [63–67], or by adjusting the relative distance of the two cavities [46,62]. The Hamiltonian of the composite system can be expressed as follows ($\hbar = 1$):

$$\begin{aligned}
\hat{H} &= \hat{H}_a + \hat{H}_b + \hat{H}_j + \hat{H}_{in},\\
\hat{H}_a &= (\omega_{a'} - i\frac{\gamma_A}{2})(\hat{a}_{cw}^\dagger \hat{a}_{cw} + \hat{a}_{ccw}^\dagger \hat{a}_{ccw}) + g_k(\hat{a}_{cw}^\dagger \hat{a}_{cw}^\dagger \hat{a}_{cw}\hat{a}_{cw} + \hat{a}_{ccw}^\dagger \hat{a}_{ccw}^\dagger \hat{a}_{ccw}\hat{a}_{ccw})\\
&\quad + \kappa_{a12}\hat{a}_{ccw}^\dagger \hat{a}_{cw} + \kappa_{a21}\hat{a}_{cw}^\dagger \hat{a}_{ccw},\\
\hat{H}_b &= (\omega_{b'} - i\frac{\gamma_B}{2})(\hat{b}_{cw}^\dagger \hat{b}_{cw} + \hat{b}_{ccw}^\dagger \hat{b}_{ccw}) + \kappa_b(\hat{b}_{cw}^\dagger \hat{b}_{ccw} + \hat{b}_{ccw}^\dagger \hat{b}_{cw}),\\
\hat{H}_j &= -iJe^{i\theta}(\hat{b}_{cw}^\dagger \hat{a}_{cw} + \hat{a}_{ccw}^\dagger \hat{b}_{ccw}),\\
\hat{H}_{in} &= \Omega(\hat{a}_{cw}^\dagger e^{-i\omega_L t} + \hat{a}_{cw} e^{i\omega_L t}).
\end{aligned} \tag{1}$$

Here, $\hat{H}_a$ ($\hat{H}_b$) describes the Hamiltonian of the cavity A (B). $\hat{a}_{cw}^\dagger$ ($\hat{a}_{cw}$) and $\hat{a}_{ccw}^\dagger$ ($\hat{a}_{ccw}$) are the creation (annihilation) operators of CW and CCW modes in cavity A, respectively. $\hat{b}_{cw}^\dagger$ ($\hat{b}_{cw}$) and $\hat{b}_{ccw}^\dagger$ ($\hat{b}_{ccw}$) are the creation (annihilation) operators of the CW and CCW modes of cavity B, respectively. $\omega_{a'} = \omega_a + \mathrm{Re}(\epsilon_1 + \epsilon_2)$, $\omega_{b'} = \omega_b + \mathrm{Re}(\kappa_b)$, ω_a (ω_b) denotes the resonance frequency of the cavity A (B), $\epsilon_{1(2)}$ represents the perturbation induced by the nanotip 1 (2). g_k is the Kerr nonlinear interaction coefficient. $\kappa_{a12(a21)} = \epsilon_1 + \epsilon_2 e^{\pm i2m\beta}$ is the scattering rate of the cavity A, which corresponds to the backscattering from the CW (CCW) mode to the CCW (CW) mode. β is the relative angle of the nanotips and m is the azimuthal mode number. κ_b is the scattering rate of the cavity B. $\gamma_A = \gamma_a - 2\mathrm{Im}(\epsilon_1 + \epsilon_2)$, $\gamma_B = \gamma_b - 2\mathrm{Im}(\kappa_b)$ are the total dissipation of cavity A and B, respectively. $\gamma_a = \gamma_{ai} + \gamma_{aex}$, $\gamma_b = \gamma_{bi} + \gamma_{bex}$, where γ_{ai} (γ_{bi}) and γ_{aex} (γ_{bex}) are the intrinsic loss and coupling loss of cavity A (B), respectively. The third term $\hat{H}_j$ describes the interaction between cavity A and B, in which $J = \sqrt{\gamma_{aex}\gamma_{bex}}$ is the coupling strength between cavity A and cavity B. Moreover, the last term $\hat{H}_{in}$ describes the driving field, and Ω is the amplitude of the monochromatic laser field. In the rotating frame at the laser frequency ω_L, the Hamiltonian of the system can be expressed as:

$$\begin{aligned}
\hat{H}' &= (\Delta_{a'} - i\frac{\gamma_A}{2})(\hat{a}_{cw}^\dagger \hat{a}_{cw} + \hat{a}_{ccw}^\dagger \hat{a}_{ccw}) + g_k(\hat{a}_{cw}^\dagger \hat{a}_{cw}^\dagger \hat{a}_{cw}\hat{a}_{cw} + \hat{a}_{ccw}^\dagger \hat{a}_{ccw}^\dagger \hat{a}_{ccw}\hat{a}_{ccw})\\
&\quad + \kappa_{a12}\hat{a}_{ccw}^\dagger \hat{a}_{cw} + \kappa_{a21}\hat{a}_{cw}^\dagger \hat{a}_{ccw}\\
&\quad + (\Delta_{b'} - i\frac{\gamma_B}{2})(\hat{b}_{cw}^\dagger \hat{b}_{cw} + \hat{b}_{ccw}^\dagger \hat{b}_{ccw}) + \kappa_b(\hat{b}_{cw}^\dagger \hat{b}_{ccw} + \hat{b}_{ccw}^\dagger \hat{b}_{cw})\\
&\quad - iJe^{i\theta}(\hat{b}_{cw}^\dagger \hat{a}_{cw} + \hat{a}_{ccw}^\dagger \hat{b}_{ccw}) + \Omega(\hat{a}_{cw}^\dagger + \hat{a}_{cw}),
\end{aligned} \tag{2}$$

where $\Delta_{a'} = \omega_a + \mathrm{Re}(\epsilon_1 + \epsilon_2) - \omega_L$ is the detuning between the driving field and the cavity A. And $\Delta_{b'} = \omega_b + \mathrm{Re}(\kappa_b) - \omega_L$ denotes the detuning between the driving field and cavity B.

The Heisenberg equations of motion for cavity B can be described as follows:

$$\begin{aligned}
\dot{\hat{b}}_{cw} &= (-i\Delta_{b'} - \frac{\gamma_B}{2})\hat{b}_{cw} - i\kappa_b \hat{b}_{ccw} - Je^{i\theta}\hat{a}_{cw}\\
\dot{\hat{b}}_{ccw} &= (-i\Delta_{b'} - \frac{\gamma_B}{2})\hat{b}_{ccw} - i\kappa_b \hat{b}_{cw}\\
\dot{\hat{b}}_{cw}^\dagger &= (i\Delta_{b'} + \frac{\gamma_B}{2})\hat{b}_{cw}^\dagger + i\kappa_b \hat{b}_{ccw}^\dagger\\
\dot{\hat{b}}_{ccw}^\dagger &= (i\Delta_{b'} + \frac{\gamma_B}{2})\hat{b}_{ccw}^\dagger + i\kappa_b \hat{b}_{cw}^\dagger + Je^{i\theta}\hat{a}_{ccw}^\dagger.
\end{aligned} \tag{3}$$

Here we assume that cavity B is dissipative, that is, cavity B can reach steady-state quickly. Then we have the relations as $\dot{\hat{b}}_{cw} = 0$, $\dot{\hat{b}}_{ccw} = 0$, $\dot{\hat{b}}_{cw}^\dagger = 0$ and $\dot{\hat{b}}_{ccw}^\dagger = 0$. Therefore, the creation operators and the annihilation operators in cavity B can be replaced by the operators in cavity A,

Optics EXPRESS

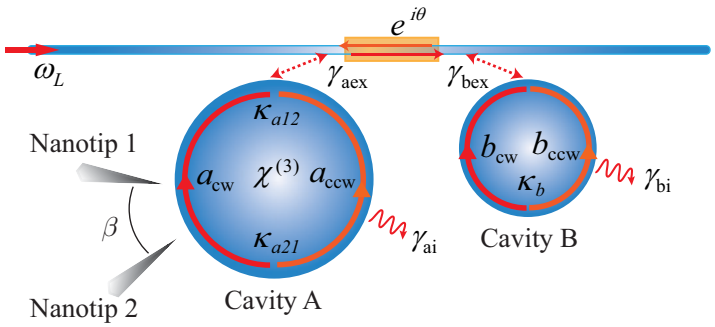

Fig. 1. Schematic of the indirectly coupled resonators system. Cavity A is driven by the pumping fields with frequency ω_L. The dissipation of cavity B is much greater than the dissipation of cavity A.

namely

$$\begin{aligned}
\hat{b}_{cw} &= \frac{iJ(\Delta_{b'} - i\frac{\gamma_B}{2})e^{i\theta}}{(\Delta_{b'} - i\frac{\gamma_B}{2})^2 - \kappa_b^2}\hat{a}_{cw},\\
\hat{b}_{ccw} &= \frac{-iJ\kappa_b e^{i\theta}}{(\Delta_{b'} - i\frac{\gamma_B}{2})^2 - \kappa_b^2}\hat{a}_{cw},\\
\hat{b}^{\dagger}_{cw} &= \frac{-iJ\kappa_b e^{i\theta}}{(\Delta_{b'} - i\frac{\gamma_B}{2})^2 - \kappa_b^2}\hat{a}^{\dagger}_{ccw},\\
\hat{b}^{\dagger}_{ccw} &= \frac{iJ(\Delta_{b'} - i\frac{\gamma_B}{2})e^{i\theta}}{(\Delta_{b'} - i\frac{\gamma_B}{2})^2 - \kappa_b^2}\hat{a}^{\dagger}_{ccw}.
\end{aligned} \tag{4}$$

The Hamiltonian of the system can be described by

$$\begin{aligned}
\hat{H}_{eff} = {} & (\Delta_{a'} - i\frac{\gamma_A}{2})(\hat{a}^{\dagger}_{cw}\hat{a}_{cw} + \hat{a}^{\dagger}_{ccw}\hat{a}_{ccw}) + g_k(\hat{a}^{\dagger}_{cw}\hat{a}^{\dagger}_{cw}\hat{a}_{cw}\hat{a}_{cw} + \hat{a}^{\dagger}_{ccw}\hat{a}^{\dagger}_{ccw}\hat{a}_{ccw}\hat{a}_{ccw})\\
& + \kappa_{a12}\hat{a}^{\dagger}_{ccw}\hat{a}_{cw} + \kappa_{a21}\hat{a}^{\dagger}_{cw}\hat{a}_{ccw} + g_b\hat{a}^{\dagger}_{ccw}\hat{a}_{cw} + \Omega(\hat{a}^{\dagger}_{cw} + \hat{a}_{cw}).
\end{aligned} \tag{5}$$

$g_b = \frac{-J^2\kappa_b e^{i2\theta}}{(\Delta_{b'} - i\frac{\gamma_B}{2})^2 - \kappa_b^2}$ is the asymmetric coupling strength between the CW and CCW modes in cavity A induced by the cavity B.

The state of the system are generally described with $|n\rangle_{cw}|s\rangle_{ccw}$, where $|n\rangle_{cw}$ and $|s\rangle_{ccw}$ are the Fock state of the CW mode and the CCW mode, respectively. Considering the few photon Fock state ($N = n + s = 2$), the eigenvalues of the system are expressed as

$$\begin{aligned}
E_0 &= 0,\\
E_1^{\pm} &= \Delta_A \pm \sigma_1,\\
E_2^{0,\pm} &= 2\Delta_A + 2g_k + \sigma_2^{0,\pm}.
\end{aligned} \tag{6}$$

Here $\Delta_A = \Delta_{a'} - i\gamma_A/2$, $\sigma_1 = \sqrt{\kappa_{a21}\kappa_{a12} + \kappa_{a21}g_b}$, $\sigma_2^0 = 0$, and $\sigma_2^{\pm} = -g_k \pm \sqrt{g_k^2 + 4\kappa_{a21}(\kappa_{a12} + g_b)}$. Then, the eigenvalues of the non-Hermitian systems are illustrated as a function of the angles θ and β. We choose parameters that are feasible with current experiments: $\gamma_{ai} = 2.992MHz$, $\gamma_{aex} = 5.984MHz$, $\gamma_{bi} = 131.6MHz$, $\gamma_{bex} = 434.3MHz$, $\kappa_b = (132.7 - 30.6i)MHz$ [62]; $\epsilon_1 = (1.5 - 0.1i)\gamma_a$, $\epsilon_2 = (1.4999 - 0.101489i)\gamma_a$, $m = 4$ [57], $g_k = 2\gamma_a$ and $\Omega = 0.3\gamma_a$. We focus on the condition of zero-detuning, i.e., $\Delta_{a'} = \Delta_{b'} = 0$. As shown in Fig. 2, the exceptional points appear periodically as β changes. By tuning β to $\kappa_{a21} = 0$, the energy level of the system will

Optics EXPRESS

degenerate. Interestingly, the impact of the phase angle θ on the interference loop results in a rapid shift in the energy levels near the EP.

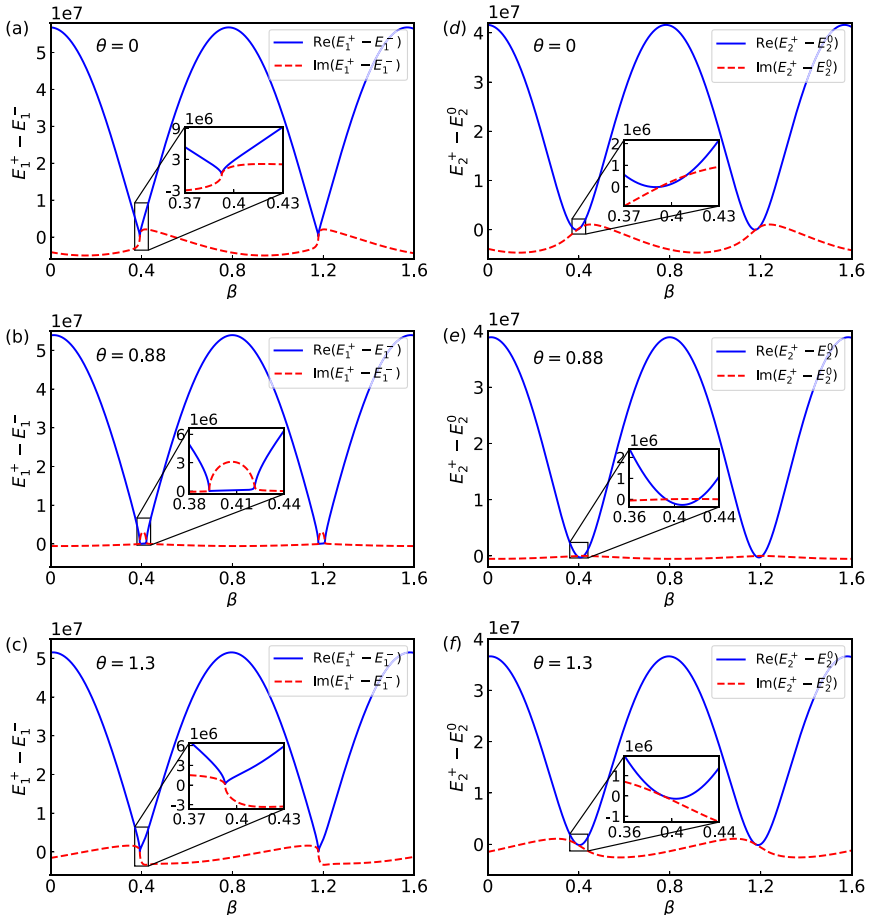

Fig. 2. Schematic diagram of the difference of the energy levels in the system at (a)-(c) N=1 and (d)-(e) N=2, when θ is at 0, 0.88, and 1.3, respectively. Here EPs appear periodically with angle β.

3. Results and discussion

The following section discusses the statistical properties of the CW mode photons in cavity A. Furthermore, the statistical properties of the mode are mainly characterized by the equal-time second-order correlation function, which could be expressed as:

$$g^{(2)}_{cw}(0) = \frac{\langle \hat{a}^{\dagger}_{cw}\hat{a}^{\dagger}_{cw}\hat{a}_{cw}\hat{a}_{cw}\rangle}{\langle \hat{a}^{\dagger}_{cw}\hat{a}_{cw}\rangle^2}. \tag{7}$$

On the condition of a weak drive ($\Omega \ll \gamma_{ai} + \gamma_{aex}$) and a small number of photons, the state can be expressed as:

$$\begin{aligned} |\psi(t)\rangle = {} & C_{00}(t)|00\rangle + C_{10}(t)|10\rangle + C_{01}(t)|01\rangle \\ & + C_{20}(t)|20\rangle + C_{11}(t)|11\rangle + C_{02}(t)|02\rangle. \end{aligned} \tag{8}$$

Optics EXPRESS

Here C_{ns} are the probability amplitudes of the state. By using the Schrödinger equation $i\frac{\partial}{\partial t}|\psi(t)\rangle = \hat{H}_{eff}|\psi(t)\rangle$, the steady-state probability amplitude can be solved as

$$\begin{aligned}
C_{00} &= 1, \\
C_{10} &= \frac{\Delta_A \Omega}{\zeta}, \\
C_{01} &= \frac{-\Omega(\kappa_{a12} + g_b)}{\zeta}, \\
C_{20} &= \frac{\sqrt{2}\Omega^2[\kappa_{a21} g_k(\kappa_{a12} + g_b) + 2\Delta_A^2(\Delta_A + g_k)]}{4\zeta(\zeta - \Delta_A g_k)(\Delta_A + g_k)}, \\
C_{11} &= -\frac{\Omega^2(\kappa_{a12} + g_b)(2\Delta_A + g_k)}{2\zeta(\zeta - \Delta_A g_k)}, \\
C_{02} &= \frac{\sqrt{2}\Omega^2(\kappa_{a12} + g_b)^2(2\Delta_A + g_k)}{4\zeta(\Delta_A + g_k)(\zeta - \Delta_A g_k)}.
\end{aligned} \tag{9}$$

Here $\zeta = \kappa_{a21}(\kappa_{a12} + g_b) - \Delta_A^2$.

3.1. Probability distribution

From Eq. (9), the single-photon and two-photon probability distributions of the CW and CCW modes in cavity A can be obtained as

$$\begin{aligned}
P_1^{cw} &= |C_{10}|^2/P_N, \\
P_2^{cw} &= |C_{20}|^2/P_N, \\
P_1^{ccw} &= |C_{01}|^2/P_N, \\
P_2^{ccw} &= |C_{02}|^2/P_N.
\end{aligned} \tag{10}$$

Here $P_N = |C_{00}|^2 + |C_{10}|^2 + |C_{01}|^2 + |C_{20}|^2 + |C_{11}|^2 + |C_{02}|^2$ is the normalization coefficient. Additionally, $|C_{11}|^2$ could be negligible relative to $|C_{10}|^2$ and $|C_{01}|^2$. Figure 3 shows the

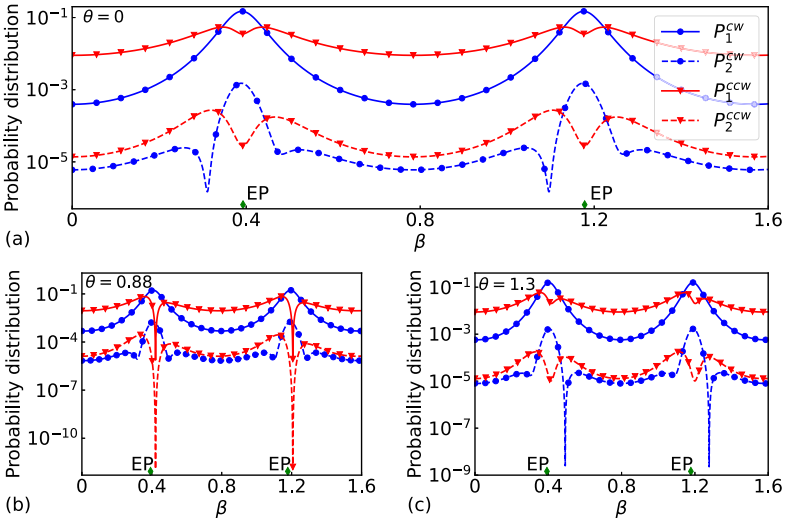

Fig. 3. Probability distributions of CW (blue) and CCW (red) modes for one-photon (solid line) and two-photon (dashed line) in cavity A, when θ is at (a) 0, (b) 0.88, and (c) 1.3.

Optics EXPRESS

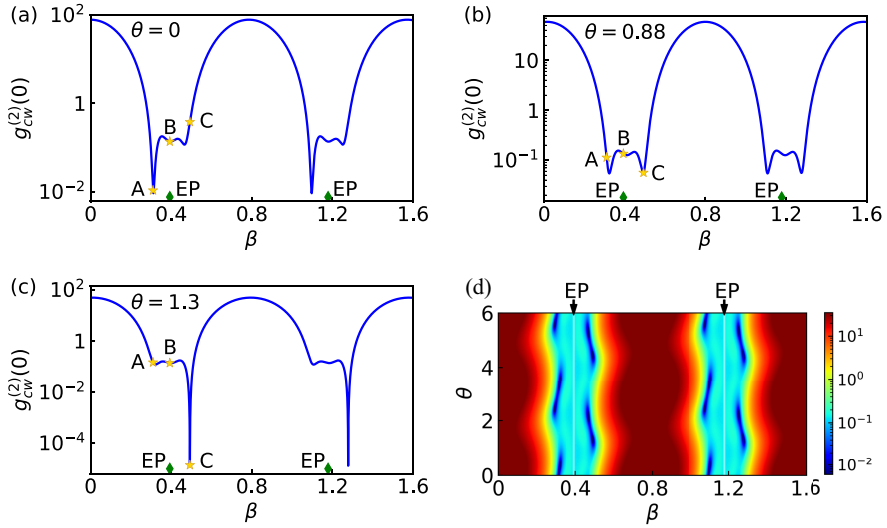

Fig. 4. Diagram of the second-order correlation function as a function of β, when θ is at (a) 0, (b) 0.88, and (c) 1.3. Here the other parameters are $\beta_A = 0.3095$, $\beta_{EPs} = \beta_B = 0.3927$, and $\beta_C = 0.4925$. (d) Diagram of the second-order correlation function as a function of β and θ. Transparent white lines represent the positions of EPs.

probability distribution of the photons as a function of the angles θ and β. When $\theta = 0$, CCW mode is suppressed at EPs, while the photons in the CW mode appear with a high probability. However, as shown in Fig. 3(b)(c), when $\theta = 0.88$ or $\theta = 1.3$, the optimal suppression point of the CCW mode is shifted due to destructive interference. Moreover, at $\theta = 0.88$, the suppression of the CCW mode is particularly obvious by tuning angle β. Simultaneously, the probability distribution of two photons in the CW mode is tuned due to the interference loop's change in the phase angle θ.

3.2. Second-order correlation function

Considering that $|C_{11}|^2$ and $|C_{20}|^2$ are far less than $|C_{10}|^2$, Eq. (7) can be approximately described as

$$g^{(2)}_{cw}(0) = \frac{\langle \hat{a}^{\dagger}_{cw}\hat{a}^{\dagger}_{cw}\hat{a}_{cw}\hat{a}_{cw}\rangle}{\langle \hat{a}^{\dagger}_{cw}\hat{a}_{cw}\rangle^2} \approx \frac{2P^{cw}_2}{(P^{cw}_1)^2}. \tag{11}$$

In Fig. 4, we show the second-order correlation function as a function of the angles θ and β. At EPs, i.e., $\beta_B = 0.3927$ as illustrated by Huang et al. [61], the energy levels of the system are degenerate, and the requirements for the two-photon resonance could be fulfilled. Meanwhile, the single-photon blockade occurs at this time. This phenomenon is exclusive to non-Hermitian systems and is independent of the angle θ. However, due to destructive interference, it is possible to detect a very strong nonconventional photon blockade near EPs after introducing a dissipative cavity with indirect coupling. Simultaneously, by changing the phase angle θ, we can tune the depth of $g^{(2)}_{cw}(0)$ at $\beta_A = 0.3095$ and $\beta_C = 0.4925$ under the condition of constant Kerr nonlinearity. As shown in Fig. 4(a),(c), when $\beta = \beta_A$, $g^{(2)}_{cw}(0)$ at $\theta = 0$ is 13.34 times lower than that at $\theta = 1.3$; when $\beta = \beta_C$, $g^{(2)}_{cw}(0)$ at $\theta = 1.3$ is 2.7×10^4 times lower than that at $\theta = 0$. In order to show the effects of angles θ and β on the statistical properties of the photons more clearly, we numerically simulate the relations and show the results in Fig. 4(d). It can be seen that the value of the second-order correlation function $g^{(2)}_{cw}(0)$ at EPs (transparent white line) does not change with the angle θ. However, especially when the quantum interference condition is

Optics EXPRESS

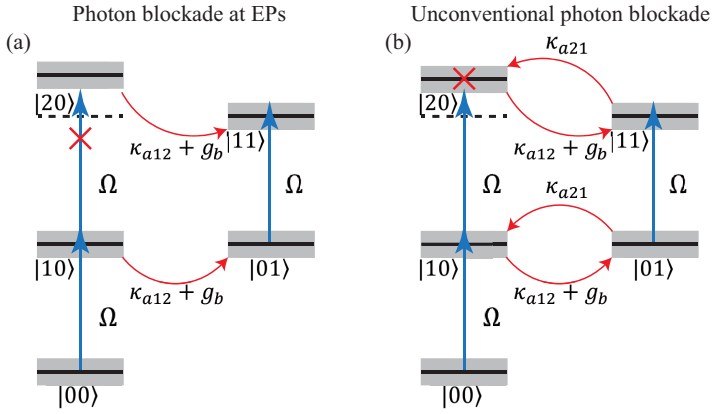

Fig. 5. Energy level diagram depicting (a) excitation paths for photon blockade at EPs and (b) interference paths are leading to unconventional photon blockade. The gray area indicates that the system energy level has a certain width.

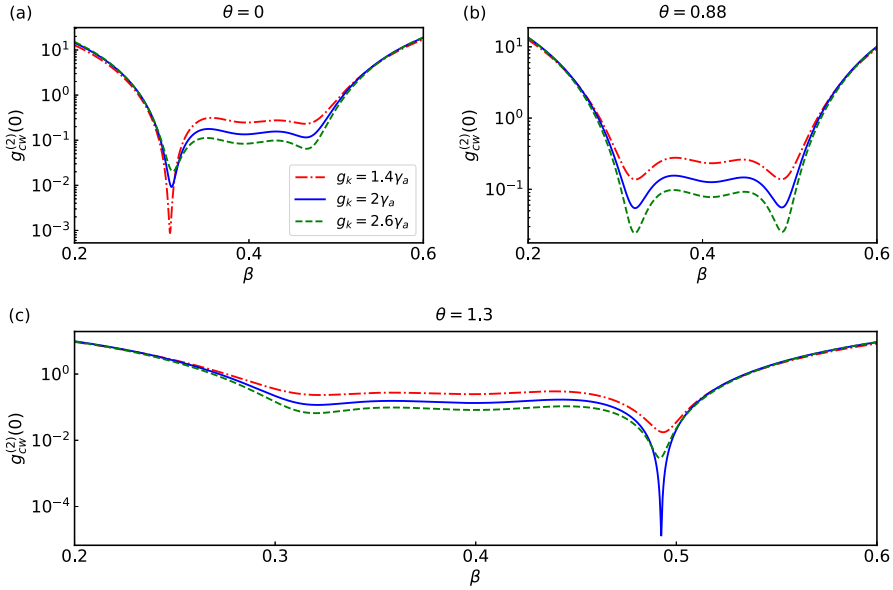

Fig. 6. Diagram of the second order correlation function as a function of β and g_k, when θ is at (a) 0, (b) 0.88, and (c) 1.3.

satisfied around EPs, the statistical features of CW mode photons in cavity A strongly depends on the angle θ. Furthermore, Fig. 5 exhibits the concept of photon blockade at EPs and the unconventional photon blockade by presenting the system's transition routes of different energy levels. The thickness of the gray area indicates the width of the energy levels in the system. It is evident that by tuning the nonlinear intensity and the interference loop, the components of the two transition pathways to the $|20\rangle$ state can be controlled. We present the results in Fig. 6 to demonstrate the constraining connection between Kerr nonlinearity and the phase angle. After choosing different nonlinear strengths, we find that the second-order correlation functions $g^{(2)}_{cw}(0)$ at $\beta_A = 0.3095$ or $\beta_C = 0.4952$ do not decrease with the increase of the nonlinearity when $\theta = 0$ or $\theta = 1.3$. Moreover, there is an optimal nonlinear strength g_k and angle θ for both A and C that

Optics EXPRESS

$g^{(2)}_{cw}(0)$ will approach zero. As shown in Fig. 5(b), when the nonlinearity g_k becomes stronger, the component of the transition path $|00\rangle \xrightarrow{\Omega} |10\rangle \xrightarrow{\Omega} |20\rangle$ decreases, and the component of the other transition path $|00\rangle \xrightarrow{\Omega} |10\rangle \xrightarrow{\kappa_{a12}+g_b} |01\rangle \xrightarrow{\Omega} |11\rangle \xrightarrow{\kappa_{a21}} |20\rangle$ are constant or increases, which results in quantum interference weakening. On the contrary, the quantum interference will also be weakened when the nonlinearity is weak. Unlike β_A and β_C, $g^{(2)}_{cw}(0)$ decreases with increasing nonlinearity at EPs [61].

Finally, the variation of $g^{(2)}_{cw}(0)$ with nonlinear strength g_k and angle θ is studied when the system parameters are chosen as $\beta_A = 0.3095$, $\beta_B = 0.3927$, and $\beta_C = 0.4925$, respectively. For the unconventional photon blockade, there is an optimal nonlinear strength and phase angle θ at β_A and β_C of the system to minimize $g^{(2)}_{cw}(0)$. As shown in Fig. 7(a),(c), when $g_k = 1.49\gamma_a$, $\theta = 3.13$, $g^{(2)}_{cw}(0)$ can reach a minimum value of 1.23×10^{-7}, which is 530 times lower than $\theta = 0$; when $g_k = 2.04\gamma_a$, $\theta = 1.297$, $g^{(2)}_{cw}(0)$ can reach a minimum value of 6×10^{-7}, which is 6×10^5

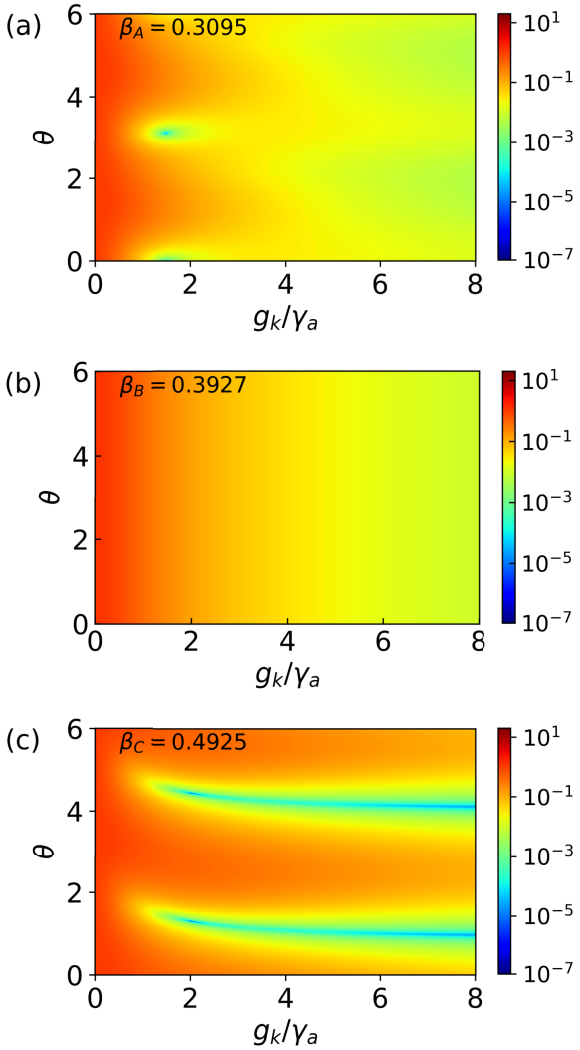

Fig. 7. Diagram of the second order correlation function as a function of θ and g_k, when the system is at (a) β_A, (b) β_B, and (c) β_C.

Optics EXPRESS

times lower than $\theta = 0$. However, as shown in Fig. 7(b), when the system is at EPs, the value of the second-order correlation function $g^{(2)}_{cw}(0)$ does not fluctuate with θ. The path interference created by the dissipative cavity can be observed to help the creation of a high-quality on-chip single-photon source.

4. Summary

In summary, we have explored the photon blockade in an indirectly coupled non-Hermitian resonators system. It is discovered that EPs still appeared regularly with the relative nanotip angle β. Nevertheless, owing to the presence of the dissipative cavity, the changes near the EPs are rapid and asymmetric, causing the energy levels of the system and the photon statistical characteristics to be highly reliant on the phase angle θ. In this approach, substantial quantum interference may be formed between the transition paths of the two-photon state, resulting in a strong anti-bunching effect. However, higher Kerr nonlinear coefficients are not always beneficial for optimal nonconventional photon blockades. Combined with the current experiment's feasible parameters, we provide the best settings for photon blockade. We believe that our results may provide a novel method for the future implementation of tunable on-chip single-photon sources.

Funding. National Natural Science Foundation of China (62071448, 62131002).

Disclosures. The authors declare no conflicts of interest.

Data availability. No data were generated or analyzed in the presented research.

References

1. A. Imamoglu, H. Schmidt, G. Woods, and M. Deutsch, "Strongly interacting photons in a nonlinear cavity," Phys. Rev. Lett. **79**(8), 1467–1470 (1997).
2. A. Faraon, I. Fushman, D. Englund, N. Stoltz, P. Petroff, and J. Vučković, "Coherent generation of non-classical light on a chip via photon-induced tunnelling and blockade," Nat. Phys. **4**(11), 859–863 (2008).
3. P. Rabl, "Photon blockade effect in optomechanical systems," Phys. Rev. Lett. **107**(6), 063601 (2011).
4. J.-Q. Liao and F. Nori, "Photon blockade in quadratically coupled optomechanical systems," Phys. Rev. A **88**(2), 023853 (2013).
5. A. Miranowicz, M. Paprzycka, Y.-x. Liu, J. C. V. Bajer, and F. Nori, "Two-photon and three-photon blockades in driven nonlinear systems," Phys. Rev. A **87**(2), 023809 (2013).
6. C. Hamsen, K. N. Tolazzi, T. Wilk, and G. Rempe, "Two-photon blockade in an atom-driven cavity qed system," Phys. Rev. Lett. **118**(13), 133604 (2017).
7. K. Wang, Y.-P. Gao, T.-T. Pang, T.-J. Wang, and C. Wang, "Enhanced photon blockade in quadratically coupled optomechanical system," EPL **131**(2), 24003 (2020).
8. D.-Y. Wang, C.-H. Bai, S. Liu, S. Zhang, and H.-F. Wang, "Photon blockade in a double-cavity optomechanical system with nonreciprocal coupling," New J. Phys. **22**(9), 093006 (2020).
9. T. C. H. Liew and V. Savona, "Single photons from coupled quantum modes," Phys. Rev. Lett. **104**(18), 183601 (2010).
10. M. Bamba, A. Imamoğlu, I. Carusotto, and C. Ciuti, "Origin of strong photon antibunching in weakly nonlinear photonic molecules," Phys. Rev. A **83**(2), 021802 (2011).
11. H. Z. Shen, Y. H. Zhou, and X. X. Yi, "Tunable photon blockade in coupled semiconductor cavities," Phys. Rev. A **91**(6), 063808 (2015).
12. H. Flayac and V. Savona, "Unconventional photon blockade," Phys. Rev. A **96**(5), 053810 (2017).
13. H. J. Snijders, J. A. Frey, J. Norman, H. Flayac, V. Savona, A. C. Gossard, J. E. Bowers, M. P. van Exter, D. Bouwmeester, and W. Löffler, "Observation of the unconventional photon blockade," Phys. Rev. Lett. **121**(4), 043601 (2018).
14. B. Li, R. Huang, X. Xu, A. Miranowicz, and H. Jing, "Nonreciprocal unconventional photon blockade in a spinning optomechanical system," Photonics Res. **7**(6), 630–641 (2019).
15. Y.-P. Gao, C. Cao, P.-F. Lu, and C. Wang, "Phase-controlled photon blockade in optomechanical systems," Fundamental Research (2022).
16. K. Wang, Y.-P. Gao, R. Jiao, and C. Wang, "Recent progress on optomagnetic coupling and optical manipulation based on cavity-optomagnonics," Front. Phys. **17**(4), 42201 (2022).
17. V. Braginsky, M. Gorodetsky, and V. Ilchenko, "Quality-factor and nonlinear properties of optical whispering-gallery modes," Phys. Lett. A **137**(7-8), 393–397 (1989).
18. L. Collot, V. Lefèvre-Seguin, M. Brune, J. M. Raimond, and S. Haroche, "Very high-q whispering-gallery mode resonances observed on fused silica microspheres," Europhys. Lett. **23**(5), 327–334 (1993).

Optics EXPRESS

19. M. L. Gorodetsky, A. A. Savchenkov, and V. S. Ilchenko, "Ultimate q of optical microsphere resonators," Opt. Lett. **21**(7), 453–455 (1996).
20. D. K. Armani, T. J. Kippenberg, S. M. Spillane, and K. J. Vahala, "Ultra-high-q toroid microcavity on a chip," Nature **421**(6926), 925–928 (2003).
21. M. Hossein-Zadeh and K. J. Vahala, "Free ultra-high-q microtoroid: a tool for designing photonic devices," Opt. Express **15**(1), 166–175 (2007).
22. A. A. Savchenkov, A. B. Matsko, V. S. Ilchenko, and L. Maleki, "Optical resonators with ten million finesse," Opt. Express **15**(11), 6768–6773 (2007).
23. M. Pöllinger, D. O'Shea, F. Warken, and A. Rauschenbeutel, "Ultrahigh-q tunable whispering-gallery-mode microresonator," Phys. Rev. Lett. **103**(5), 053901 (2009).
24. M. Sumetsky, Y. Dulashko, and R. S. Windeler, "Optical microbubble resonator," Opt. Lett. **35**(7), 898–900 (2010).
25. L. Wu, H. Wang, Q. Yang, Q. xin Ji, B. Shen, C. Bao, M. Gao, and K. Vahala, "Greater than one billion q factor for on-chip microresonators," Opt. Lett. **45**(18), 5129–5131 (2020).
26. Z. Shen, Y.-L. Zhang, Y. Chen, C.-L. Zou, Y.-F. Xiao, X.-B. Zou, F.-W. Sun, G.-C. Guo, and C.-H. Dong, "Experimental realization of optomechanically induced non-reciprocity," Nat. Photonics **10**(10), 657–661 (2016).
27. X.-F. Liu, T.-J. Wang, Y.-P. Gao, C. Cao, and C. Wang, "Chiral microresonator assisted by rydberg-atom ensembles," Phys. Rev. A **98**(3), 033824 (2018).
28. Y. Sun, X.-F. Liu, T.-J. Wang, and Y.-P. Gao, "Photothermally induced transparency in mode-cascaded microcavity," Adv. Photonics Res. **1**(2), 2000016 (2020).
29. K. Djordjev, S.-J. Choi, S.-J. Choi, and R. Dapkus, "Microdisk tunable resonant filters and switches," IEEE Photonics Technol. Lett. **14**(6), 828–830 (2002).
30. A. Savchenkov, V. Ilchenko, A. Matsko, and L. Maleki, "High-order tunable filters based on a chain of coupled crystalline whispering gallery-mode resonators," IEEE Photonics Technol. Lett. **17**(1), 136–138 (2005).
31. D. Kwon, D. Jeong, I. Jeon, H. Lee, and J. Kim, "Ultrastable microwave and soliton-pulse generation from fibre-photonic-stabilized microcombs," Nat. Commun. **13**(1), 381 (2022).
32. L. Yao, P. Liu, H.-J. Chen, Q. Gong, Q.-F. Yang, and Y.-F. Xiao, "Soliton microwave oscillators using oversized billion q optical microresonators," Optica **9**(5), 561–564 (2022).
33. J. Zhu, S. K. Ozdemir, Y.-F. Xiao, L. Li, L. He, D.-R. Chen, and L. Yang, "On-chip single nanoparticle detection and sizing by mode splitting in an ultrahigh-q microresonator," Nat. Photonics **4**(1), 46–49 (2010).
34. J. Liao and L. Yang, "Optical whispering-gallery mode barcodes for high-precision and wide-range temperature measurements," Light: Sci. Appl. **10**(1), 32 (2021).
35. Y. Wan, X. Fan, B. Xu, and Z. He, "Microwave frequency measurement with high accuracy and wide bandwidth based on whispering-gallery mode barcode," Opt. Lett. **46**(19), 5008–5011 (2021).
36. T. Siegle, S. Schierle, S. Kraemmer, B. Richter, S. F. Wondimu, P. Schuch, C. Koos, and H. Kalt, "Photonic molecules with a tunable inter-cavity gap," Light: Science & Applications **6**(3), e16224 (2017).
37. K. Liao, X. Hu, T. Gan, Q. Liu, Z. Wu, C. Fan, X. Feng, C. Lu, Y. chun Liu, and Q. Gong, "Photonic molecule quantum optics," Adv. Opt. Photonics **12**(1), 60–134 (2020).
38. A. Naweed, G. Farca, S. I. Shopova, and A. T. Rosenberger, "Induced transparency and absorption in coupled whispering-gallery microresonators," Phys. Rev. A **71**(4), 043804 (2005).
39. K. Totsuka, N. Kobayashi, and M. Tomita, "Slow light in coupled-resonator-induced transparency," Phys. Rev. Lett. **98**(21), 213904 (2007).
40. X.-W. Xu and Y. Li, "Strong photon antibunching of symmetric and antisymmetric modes in weakly nonlinear photonic molecules," Phys. Rev. A **90**(3), 033809 (2014).
41. M. Zhang, C. Wang, Y. Hu, A. Shams-Ansari, T. Ren, S. Fan, and M. Lončar, "Electronically programmable photonic molecule," Nat. Photonics **13**(1), 36–40 (2019).
42. Q. Xu, S. Sandhu, M. L. Povinelli, J. Shakya, S. Fan, and M. Lipson, "Experimental realization of an on-chip all-optical analogue to electromagnetically induced transparency," Phys. Rev. Lett. **96**(12), 123901 (2006).
43. Y.-F. Xiao, V. Gaddam, and L. Yang, "Coupled optical microcavities: an enhanced refractometric sensing configuration," Opt. Express **16**(17), 12538–12543 (2008).
44. Y.-F. Xiao, M. Li, Y.-C. Liu, Y. Li, X. Sun, and Q. Gong, "Asymmetric fano resonance analysis in indirectly coupled microresonators," Phys. Rev. A **82**(6), 065804 (2010).
45. W. Li, H. Zhang, P. Han, X. Chang, S. Jiang, Y. Zhou, A. Huang, and Z. Xiao, "Real frequency splitting indirectly coupled anti-parity-time symmetric nanoparticle sensor," J. Appl. Phys. **128**(13), 134503 (2020).
46. B.-B. Li, Y.-F. Xiao, C.-L. Zou, X.-F. Jiang, Y.-C. Liu, F.-W. Sun, Y. Li, and Q. Gong, "Experimental controlling of fano resonance in indirectly coupled whispering-gallery microresonators," Appl. Phys. Lett. **100**(2), 021108 (2012).
47. Z.-H. Peng, C.-X. Jia, Y.-Q. Zhang, J.-B. Yuan, and L.-M. Kuang, "Level attraction and pt symmetry in indirectly coupled microresonators," Phys. Rev. A **102**(4), 043527 (2020).
48. C. M. Bender and S. Boettcher, "Real spectra in non-hermitian hamiltonians having pt symmetry," Phys. Rev. Lett. **80**(24), 5243–5246 (1998).
49. C. M. Bender, "Making sense of non-hermitian hamiltonians," Rep. Prog. Phys. **70**(6), 947–1018 (2007).
50. V. V. Konotop, J. Yang, and D. A. Zezyulin, "Nonlinear waves in $\mathcal{PT}$-symmetric systems," Rev. Mod. Phys. **88**(3), 035002 (2016).

Optics EXPRESS

51. L. Feng, R. El-Ganainy, and L. Ge, "Non-hermitian photonics based on parity–time symmetry," Nat. Photonics **11**(12), 752–762 (2017).
52. S. Longhi, "Parity-time symmetry meets photonics: A new twist in non-hermitian optics," EPL **120**(6), 64001 (2017).
53. J. Zhang, B. Peng, Ş. K. Özdemir, K. Pichler, D. O. Krimer, G. Zhao, F. Nori, Y.-X. Liu, S. Rotter, and L. Yang, "A phonon laser operating at an exceptional point," Nat. Photonics **12**(8), 479–484 (2018).
54. C. Wang, W. R. Sweeney, A. D. Stone, and L. Yang, "Coherent perfect absorption at an exceptional point," Science **373**(6560), 1261–1265 (2021).
55. J. Wiersig, "Enhancing the sensitivity of frequency and energy splitting detection by using exceptional points: Application to microcavity sensors for single-particle detection," Phys. Rev. Lett. **112**(20), 203901 (2014).
56. J. Wiersig, "Sensors operating at exceptional points: General theory," Phys. Rev. A **93**(3), 033809 (2016).
57. B. Peng, S. K. Özdemir, M. Liertzer, W. Chen, J. Kramer, H. Yilmaz, J. Wiersig, S. Rotter, and L. Yang, "Chiral modes and directional lasing at exceptional points," Proc. Natl. Acad. Sci. **113**(25), 6845–6850 (2016).
58. Y.-P. Gao, C. Cao, Y.-W. Duan, X.-F. Liu, T.-T. Pang, T.-J. Wang, and C. Wang, "Magnons scattering induced photonic chaos in the optomagnonic resonators," Nanophotonics **9**(7), 1953–1961 (2020).
59. H. Lü, C. Wang, L. Yang, and H. Jing, "Optomechanically induced transparency at exceptional points," Phys. Rev. Appl. **10**(1), 014006 (2018).
60. W.-L. Xu, Y.-P. Gao, C. Cao, T.-J. Wang, and C. Wang, "Nanoscatterer-mediated frequency combs in cavity optomagnonics," Phys. Rev. A **102**(4), 043519 (2020).
61. R. Huang, S. K. Özdemir, J.-Q. Liao, F. Minganti, L.-M. Kuang, F. Nori, and H. Jing, "Exceptional photon blockade: Engineering photon blockade with chiral exceptional points," Laser Photonics Rev. **16**(7), 2100430 (2022).
62. C. Wang, X. Jiang, G. Zhao, M. Zhang, C. W. Hsu, B. Peng, A. D. Stone, L. Jiang, and L. Yang, "Electromagnetically induced transparency at a chiral exceptional point," Nat. Phys. **16**(3), 334–340 (2020).
63. C. T. Phare, Y.-H. Daniel Lee, J. Cardenas, and M. Lipson, "Graphene electro-optic modulator with 30ghz bandwidth," Nat. Photonics **9**(8), 511–514 (2015).
64. J. Liu, G. Xu, F. Liu, I. Kityk, X. Liu, and Z. Zhen, "Recent advances in polymer electro-optic modulators," RSC Adv. **5**(21), 15784–15794 (2015).
65. K. Powell, L. Li, A. Shams-Ansari, J. Wang, D. Meng, N. Sinclair, J. Deng, M. Lončar, and X. Yi, "Integrated silicon carbide electro-optic modulator," Nat. Commun. **13**(1), 1851 (2022).
66. B. Pan, H. Cao, Y. Huang, Z. Wang, K. Chen, H. Li, Z. Yu, and D. Dai, "Compact electro-optic modulator on lithium niobate," Photonics Res. **10**(3), 697–702 (2022).
67. T. Murai, Y. shoji, and T. Mizumoto, "Light-induced thermomagnetic recording of thin-film magnet cofeb on silicon waveguide for on-chip magneto-optical memory," Opt. Express **30**(11), 18054–18065 (2022).